



Film condensation with a non-condensable gas: Hybrid integral transforms solution for external boundary layers

Kleber Marques Lisboa^{a,*}, Karoline da Costa Rocha Fernandes Ferreira^a,
Isabela Florindo Pinheiro^a, Leandro Alcoforado Sphaier^a, Renato Machado Cotta^{b,c}

^a Laboratory of Thermal Sciences (LATERMO), Department of Mechanical Engineering (TEM/PGMEC), Universidade Federal Fluminense, UFF, Niterói, RJ, Brazil

^b Laboratory of Nano & Microfluidics and Microsystems, LabMEMS, Mechanical Engineering Dept., POLI & COPPE, UFRJ, Federal University of Rio de Janeiro, Brazil

^c Nuclear and Technological Development, DGDNTM, Brazilian Navy, Ministry of Defense, RJ, Brazil

ARTICLE INFO

Keywords:

Generalized integral transform technique
External heat and fluid flow boundary layer theory
Film condensation
Non-condensable gas
Hybrid methods

ABSTRACT

The film condensation heat transfer problem in the presence of a heavy non-condensable gas is revisited. To provide an accurate and robust hybrid numerical-analytical treatment, a systematic framework for solving heat and fluid flow described by boundary layer formulations via integral transforms has been proposed. A physically inspired change of variables stemming from the scale analysis of the governing equations is employed, aiming at facilitating algebraic manipulations and improving the convergence behavior of the Generalized Integral Transform Technique (GITT) hybrid solution. The boundary layer model for condensation processes with non-condensing substances, along with the developed solution method, are verified through comparisons with the Karman-Pohlhausen integral method and experimental results from the literature. The agreement is overall satisfactory, building confidence on the proposed methodology and computational code. In addition, a physical analysis further confirms the marked effect the non-condensable gas has on the condensation process, in some cases, decreasing the heat transfer rate by more than 80% when compared to the case with pure vapor. Interestingly, the heat transfer rate is determined to hold the same scaling with the height of the wall predicted by the classical Nusselt model for condensation of saturated pure vapor. In contrast, the temperature difference between the gas mixture and the wall, which is the driving force of the process, partially loses the strong effect predicted by the Nusselt model due to the build-up of non-condensable gas at the interface and the associated decrease in local vapor pressure.

1. Introduction

Heterogeneous condensation occurs when a gaseous phase of a particular substance contacts a surface whose temperature is sufficiently below the saturation temperature to induce phase change [1]. This physical process is widely present in industry, with applications in heat pipes [2,3], nuclear reactor design [4,5], water desalination and harvesting [6,7], among others.

Two main modes of heterogeneous condensation have been identified, namely film- and dropwise condensation [1]. The former is characterized by the formation of a continuous condensate film adjacent to the cold surface, acting as a heat transfer intermediary between the vapor and the wall. On the other hand, in dropwise condensation, several droplets form along the cold surface, coalesce, and then move, freeing space for the nucleation of new droplets. Whether film- or

dropwise condensation will occur is intimately related to the condensate wettability on a particular surface, with high contact angles and low surface energies favoring the latter [8–10].

Given the comparatively more favorable thermophysical properties of the liquid phase, one might think film condensation is preferable as far as improving heat transfer is concerned. However, the presence of the condensate film adds another thermal resistance, further hindering the flow of energy from the bulk vapor to the solid surface. In dropwise condensation, a considerable portion of the surface is directly exposed to the vapor, thereby leading to heat transfer coefficients up to 7 times higher than film condensation under similar circumstances [9,10]. Even though many efforts have been devoted to harness dropwise condensation in industrial applications, its use still suffers from higher costs and long-term degradation of the surface hydrophobicity [1,9,10]. Therefore, adopting film condensation can be considered a conservative hypothesis when designing heat transfer equipment.

* Corresponding author.

E-mail address: kmlisboa@id.uff.br (K.M. Lisboa).

<https://doi.org/10.1016/j.ijthermalsci.2023.108648>

Received 13 February 2022; Received in revised form 14 June 2023; Accepted 6 September 2023

Available online 18 September 2023

1290-0729/© 2023 Elsevier Masson SAS. All rights reserved.

Nomenclature	
$c_{p,l}$	Specific heat of the condensate
D_{vg}	Vapor diffusivity in the gas
f	Dimensionless streamfunction
F	Filter for the streamfunction
g	Gravity acceleration
h	Heat transfer coefficient
h_{fg}	Latent heat of vaporization
h_m	Average heat transfer coefficient
Ja	Jakob number
k	Thermal conductivity of the gas mixture
k_l	Thermal conductivity of the condensate
\dot{m}	Condensate mass flux
M_g	Molar mass of the non-condensable gas
M_v	Molar mass of the vapor
N	Norm
\mathcal{N}	Truncation order
Nu_m	Average Nusselt number
p	Total pressure
Pr	Prandtl number of the gas mixture
Pr_l	Prandtl number of the condensate
q_w	Wall heat flux
Q'	Heat transfer rate per unit of depth
Q'_{Nu}	Heat transfer rate per unit of depth for pure vapor
Ra_c	Concentration Rayleigh number
Sc	Schmidt number of the gas mixture
T	Temperature of the gas mixture
T_l	Temperature of the liquid film
T_w	Wall temperature
T_∞	Bulk temperature of the gas mixture
u	Vertical component of the velocity in the gas mixture
u_l	Vertical component of the velocity in the liquid film
v	Horizontal component of the velocity in the gas mixture
v_l	Horizontal component of the velocity in the liquid film
W	Mass fraction of non-condensable gas
W_∞	Bulk mass fraction of non-condensable gas
x	Vertical coordinate
y	Horizontal coordinate
<i>Greek Symbols</i>	
β_T	Thermal expansion coefficient
δ	Thickness of the condensate film
η	Modified horizontal coordinate
θ	Dimensionless temperature
λ	Eigenvalues
μ_l	Dynamic viscosity of the liquid film
ν	Kinematic viscosity of the gas mixture
ν_l	Kinematic viscosity of the liquid film
ξ	Modified vertical coordinate
ρ	Density of the gas mixture
ρ_l	Density of the condensate
φ	Modified mass fraction
ψ	Eigenfunctions
Ψ	Streamfunction
<i>Superscripts and subscripts</i>	
f	Related to the streamfunction
F	Filter
i	At the interface
m, n, q	Indexes for the eigenfunctions and eigenvalues
θ	Related to the temperature
φ	Related to the mass fraction
*	Filtered quantity
\sim	Normalized quantity
–	Transformed quantity

Othmer [11] was the first to note that the presence of a non-condensable gas mixed with the vapor markedly reduces the heat transfer rate, with 50% lower values being obtained with a gas mixture containing just 0.5 vol% of air in water vapor. This figure was further confirmed by several experimental [4,12,13] and theoretical [5,14–17] works that followed. The physical mechanism involved is the accumulation of non-condensable gas at the interface between the gas mixture and the condensate, shielding the vapor from this location, and thus reducing the local vapor pressure [14,15]. In engineering applications, the presence of non-condensables is unavoidable, either since the start of operation, due to remaining amounts of these substances, or later, due to diffusion and mixing of gases from external sources with the vapor. Indeed, loss of coolant accident (LOCA) scenarios required in the design and licensing of nuclear power plants containment buildings [4,5] and some water desalination equipment [6] may deal with gas mixtures composed majorly of non-condensable gases. In sum, given the possible dramatic effects on heat transfer, studying the consequences of the presence of a non-condensable gas during condensation is of paramount importance.

The advent of Computational Fluid Dynamics (CFD) has expanded the applicability of theoretical analyses of fluid flows far beyond what approximate analytical methods could achieve. Nonetheless, analytical methods offer unmatched accuracy and low computational cost when compared with purely numerical alternatives. In the last four decades, hybrid methods, aiming at combining the desirable features of both numerical and analytical methods, were developed. One such method is the Generalized Integral Transform Technique (GITT) [18–20], a hybrid method that extends the Classical Integral Transform Technique (CITT)

[21] to *a priori* non-transformable problems. Most of the workload in the implementation of this approach is conducted analytically, with typically only a system of coupled ordinary differential equations being solved numerically, leveraging the availability of numerical solvers with automatic error control for this task. This feature of the GITT has enabled its application in the solution of a wide range of problems involving moving boundaries [22], variable thermophysical properties [23], irregular geometries [24–26], heat and mass transfer in porous media [27,28], chemically reacting systems [29], conjugate convection-conduction-radiation heat transfer [30], among others.

In fluid flow analysis, the GITT has been extended to deal with both Navier-Stokes [23,31] and boundary layer [32,33] equations in either primitive variables or streamfunction-only formulations. However, the efforts involving boundary layers were mostly focused on internal flows, which allowed for the imposition of a second physical boundary condition to the transversal component of the velocity vector and the employment of fourth-order eigenvalue problems with superior convergence behavior [32,33]. External boundary layers for heat and fluid flow were also addressed in a few contributions [34–37], but so far, no systematic approach to solve these problems through the GITT has been reported, especially when complex phenomena beyond convection-diffusion are present. In this scenario, this work is also aimed at presenting a framework for the analysis of external boundary layer formulations using the GITT. Film condensation in the presence of a non-condensable gas is indeed a challenging case study to demonstrate the accuracy and robustness of the proposed hybrid approach, besides carrying an intrinsic importance to industrial applications. This problem is in fact challenging even for purely numerical methods, often requiring

that the condensate film thickness be neglected, avoiding multiphase flow analyses and the associated moving boundary [5,17]. In the current analysis, external boundary layer formulations for mass, momentum, energy, and species conservation are directly solved and the results are compared with approximate and experimental results, followed by a brief physical analysis.

2. Model and methods

Fig. 1 illustrates a saturated mixture composed of a condensable and a non-condensable gas with temperature T_∞ , pressure p , and non-condensable gas mass fraction W_∞ that interacts with a cold vertical wall at uniform temperature T_w . Upon this contact, a condensate film forms adjacent to the wall and flows downward due to gravity. The portions of the gas mixture sufficiently far from the wall are assumed quiescent, thus the pressure variation along the x -direction is determined according to hydrostatic principles. The gas mixture layers in the vicinity of the interface with the film are dragged by the liquid. In addition, buoyancy forces act on the gas mixture because of temperature and concentration gradients induced by the condensation process. Finally, the flow is assumed to be in steady state and two-dimensional.

2.1. Condensate film model and solution

The same hypotheses proposed by Nusselt's model for the condensate film are adopted, i.e., boundary layer equations with negligible inertial/convective effects [38]. The presence of the non-condensable gas along with the resulting dramatic drop in condensation rate tend to render these assumptions even more accurate than for the analysis of pure vapor condensation [14,15]. The reduced condensation rate results in liquid films less than 100 μm thick and a Reynolds number based on the film thickness below 10, well within the laminar flow range.

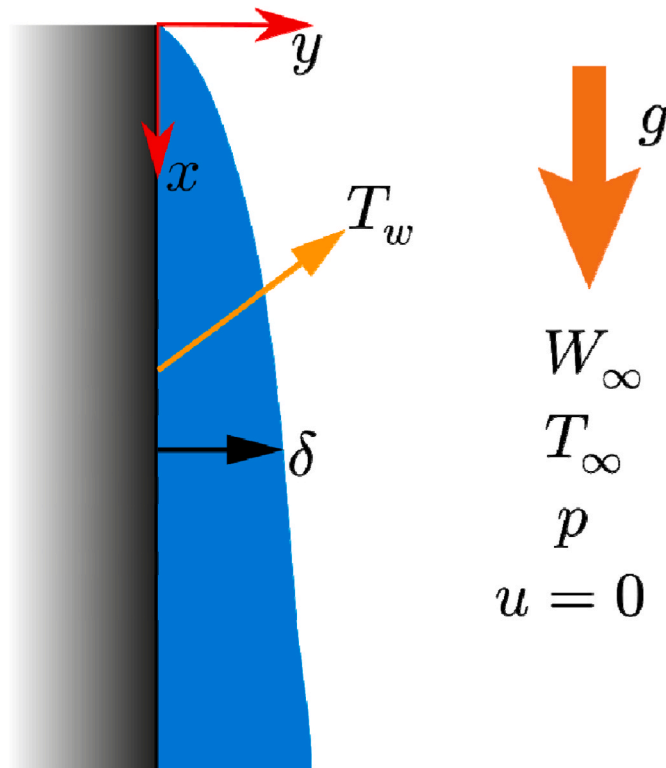


Fig. 1. Illustration of the film condensation on a vertical wall in the presence of a non-condensable gas. Condensate film indicated in blue and with thickness $\delta(x)$. Uniform wall temperature T_w . Bulk gas mixture properties are also included. A Cartesian coordinate system is indicated in red.

Furthermore, the adoption of the boundary layer hypothesis allows for the assumption of constant pressure along the y -direction, thus resulting in a buoyancy force per unit of volume acting on the liquid film given by $(\rho_l - \rho)g$, where ρ_l and ρ are the densities of the liquid and the bulk gas mixture, respectively. Assuming $\rho_l \gg \rho$, one can then approximate the buoyancy force per unit of volume by $\rho_l g$. With these simplifications, together with the assumption of constant properties, the mass, momentum, and energy conservation principles for the condensate film can then be written as,

$$\frac{\partial u_l}{\partial x} + \frac{\partial v_l}{\partial y} = 0 \quad (1.a)$$

$$\nu_l \frac{\partial^2 u_l}{\partial y^2} + g = 0 \quad (1.b)$$

$$k_l \frac{\partial^2 T_l}{\partial y^2} = 0 \quad (1.c)$$

with boundary conditions given by,

$$u_l(x, 0) = v_l(x, 0) = 0 \quad (1.d,e)$$

$$\mu_l \left. \frac{\partial u_l}{\partial y} \right|_{y=\delta} \cong 0 \quad (1.f)$$

$$T_l(x, 0) = T_w; \quad T_l(x, \delta) = T_i \quad (1.g,h)$$

where u_l and v_l are the velocity components of the condensate film in the x - and y -directions, respectively, T_l is the temperature of the condensate, T_w is the wall temperature, T_i is the temperature of the interface, ν_l is the kinematic viscosity of the condensate, μ_l is the dynamic viscosity of the condensate, k_l is the thermal conductivity of the condensate, and δ is the thickness of the condensate film. Eq. (1.f) considers that interfacial shear is small, which is supported by the limited effect it has on condensation heat transfer [39].

Analytical solutions for eqs. (1.a-h) are attainable in terms of the *a priori* unknown film thickness, δ , and interfacial temperature, T_i , as follows,

$$u_l(x, y) = \frac{g\delta^2}{\nu_l} \frac{y}{\delta} \left(1 - \frac{1}{2} \frac{y}{\delta} \right) \quad (2.a)$$

$$v_l(x, y) = -\frac{g\delta^2}{2\nu_l} \delta'(x) \left(\frac{y}{\delta} \right)^2 \quad (2.b)$$

$$T_l(x, y) = T_w + (T_i - T_w) \frac{y}{\delta} \quad (2.c)$$

Moreover, employing a mass balance at the interface, eqs. (2.a,b) can be used to establish a relation between the film thickness and the condensate mass flux into the liquid film in the form,

$$\dot{m}'' = [\rho_l u_l \delta'(x) - \rho_l v_l]_{y=\delta} = \frac{\rho_l g \delta^2}{\nu_l} \delta'(x) \quad (3)$$

where \dot{m}'' is the mass flux of condensate into the film per unit of wall area.

2.2. Gas mixture boundary layer

Temperature and mass fraction gradients are induced by the condensation process, leading to appreciable buoyancy forces and, therefore, natural convection in the gas mixture. Instead of accounting for variable thermophysical properties in full, the Boussinesq approximation is adopted for the buoyancy forces associated with both thermal- and concentration-induced density variations [14,16]. Otherwise, the thermophysical properties are assumed constant. A binary condensable-non-condensable gas mixture is considered. The boundary

layer hypothesis is adopted, consequently leading to a negligible pressure variation along y and a negligible diffusivity along the vertical direction as well. Also, the non-condensable gas molecules are assumed to be heavier than the condensable ones. These simplifications lead to the following relations for the mass, momentum, energy, and species conservation principles in the gas mixture:

$$\frac{\partial u}{\partial x} + \frac{\partial v}{\partial y} = 0 \quad (4.a)$$

$$u \frac{\partial u}{\partial x} + v \frac{\partial u}{\partial y} = \nu \frac{\partial^2 u}{\partial y^2} + g\beta_c(W - W_\infty) - g\beta_T(T - T_\infty) \quad (4.b)$$

$$u \frac{\partial T}{\partial x} + v \frac{\partial T}{\partial y} = \alpha \frac{\partial^2 T}{\partial y^2} \quad (4.c)$$

$$u \frac{\partial W}{\partial x} + v \frac{\partial W}{\partial y} = D_{vg} \frac{\partial^2 W}{\partial y^2} \quad (4.d)$$

with boundary conditions given by,

$$u(0, y) = 0 \quad (4.e)$$

$$T(0, y) = T_\infty \quad (4.f)$$

$$W(0, y) = W_\infty \quad (4.g)$$

$$u(x, \delta) = u_i(x, \delta) \quad (4.h)$$

$$\dot{m}'' = [\rho u \delta'(x) - \rho v]_{y=\delta} \quad (4.i)$$

$$u(x, y \rightarrow \infty) = 0 \quad (4.j)$$

$$T(x, \delta) = T_i; \quad T(x, y \rightarrow \infty) = T_\infty \quad (4.k,l)$$

$$\dot{m}'' W(x, \delta) + \rho D_{vg} \left. \frac{\partial W}{\partial y} \right|_{y=\delta} = 0 \quad (4.m)$$

$$W(x, y \rightarrow \infty) = W_\infty \quad (4.n)$$

and,

$$\beta_c = \frac{M_g - M_v}{M_g - (M_g - M_v)W_\infty} \quad (4.o)$$

where u and v are the velocity components of the gas mixture in the x - and y -directions, respectively, T is the temperature of the gas mixture, W is the mass fraction of the non-condensable gas, ν is the kinematic viscosity of the gas mixture, T_∞ and W_∞ are the temperature and mass fraction of the non-condensable gas in the bulk gas mixture, respectively, $\beta_T \equiv 1/T_\infty$ is the thermal expansion coefficient of the gas mixture, α is the thermal diffusivity of the gas mixture, D_{vg} is the vapor diffusivity in the gas, M_g is the molar mass of the non-condensable gas, and M_v is the molar mass of the condensable gas (vapor). The boundary condition of eq. (4.i) stems from a mass balance at the interface on the gas mixture side and serves as a boundary condition for v , while eq. (4.m) stems from the assumed impermeability of the liquid film to the non-condensable gas.

2.3. Energy balance at the interface and antoine equation

By employing an energy balance at the interface between the liquid film and the gas mixture, one can propose a condensate film growth model as follows,

$$\dot{m}'' h_{fg} - k_l \left. \frac{\partial T_l}{\partial y} \right|_{y=\delta} = -k \left. \frac{\partial T}{\partial y} \right|_{y=\delta} \quad (5)$$

where h_{fg} is the latent heat of vaporization of the condensing substance, and k is the thermal conductivity of the gas mixture.

Finally, to achieve closure for the models presented so far, it is necessary to connect the temperature at the interface, T_i , to the local vapor pressure, and, consequently, to the mass fraction of non-condensable gas at this location. For this purpose, the Antoine equation is used to relate the vapor pressure and the saturation temperature [40]. Naturally, it is assumed that, at the interface, the condensing substance is saturated. Employing the state equation for ideal gases, Dalton's law, and rearranging, yields,

$$T_i = \frac{3816.44}{23.1964 - \ln\left(\frac{M_g(1 - W_i)}{M_g(1 - W_i) + M_v W_i P}\right)} - 227.02 \quad (6)$$

where $W_i \equiv W(x, \delta)$ is the mass fraction of non-condensable gas at the interface. With the numerical values of eq. (6), the pressure must be in Pa and the temperature in °C.

2.4. Generalized Integral Transform Technique (GITT)

2.4.1. Change of variables

Previous contributions involving integral transforms solutions to external boundary layers have opted for primitive variables formulations [34–37]. However, GITT is known to greatly benefit from the introduction of as much physical information as possible into the solution process [18–20]. A scale analysis of natural convection boundary layer models can show that flow variables such as the vertical velocity component and the thickness of the boundary layer scale with $x^{1/2}$ and $x^{1/4}$, respectively [41]. Although, in general, these scales do not fully capture the behavior of these variables with x , their introduction could improve possible convergence and model manipulation issues. Hence, a change of variables $\{x, y\} \rightarrow \{\xi, \eta\}$, analogous to the one used for self-similar solutions and based on scale analysis of the model, is introduced as follows,

$$\xi \equiv x; \quad \eta \equiv (y - \delta)\zeta x^{-1/4} \quad (7.a,b)$$

and,

$$\Psi \equiv D_{vg} \zeta^2 \xi^{3/4} f(\xi, \eta) \quad (7.c)$$

$$\zeta \equiv \left[\frac{g\beta_c}{\nu D_{vg}} \right]^{1/4} \quad (7.d)$$

where Ψ is the streamfunction and f is a dimensionless streamfunction. Note that, differently from similarity solution procedures, f is not assumed to vary only with η . Similar scale-analysis-based change of variables can be introduced for any boundary layer problem [41], though they might differ to some extent from eqs. (7.a-d).

Employing the usual definition of the streamfunction and the set of variables presented in eqs. (7.a-d), one may then write the dependent variables of the mixture as,

$$u = \frac{\partial \Psi}{\partial y} = D_{vg} \zeta^2 \xi^{1/2} \frac{\partial f}{\partial \eta} \quad (8.a)$$

$$v = -\frac{\partial \Psi}{\partial x} = D_{vg} \zeta \left\{ \delta'(\xi) \zeta \xi^{1/2} \frac{\partial f}{\partial \eta} - \xi^{3/4} \frac{\partial f}{\partial \xi} + \left[\frac{\eta}{4} \frac{\partial f}{\partial \eta} - \frac{3}{4} f \right] \xi^{-1/4} \right\} \quad (8.b)$$

$$\theta = \frac{T - T_\infty}{T_w - T_\infty} \quad (8.c)$$

$$\varphi = W - W_\infty \quad (8.d)$$

Finally, introducing eqs. (8.a-d) into eqs. (4.a-n), rearranging, and simplifying yields,

$$\begin{aligned} \xi \left[\frac{\partial f}{\partial \eta} \frac{\partial^2 f}{\partial \xi \partial \eta} - \frac{\partial f}{\partial \xi} \frac{\partial^2 f}{\partial \eta^2} \right] - \frac{3}{4} f \frac{\partial^2 f}{\partial \eta^2} + \frac{1}{2} \left(\frac{\partial f}{\partial \eta} \right)^2 \\ = Sc \frac{\partial^3 f}{\partial \eta^3} + Sc \varphi + Sc \frac{\beta_T}{\beta_c} (T_\infty - T_w) \theta \end{aligned} \quad (9.a)$$

$$\xi \left[\frac{\partial f}{\partial \eta} \frac{\partial \theta}{\partial \xi} - \frac{\partial f}{\partial \xi} \frac{\partial \theta}{\partial \eta} \right] - \frac{3}{4} f \frac{\partial \theta}{\partial \eta} = \frac{Sc}{Pr} \frac{\partial^2 \theta}{\partial \eta^2} \quad (9.b)$$

$$\xi \left[\frac{\partial f}{\partial \eta} \frac{\partial \varphi}{\partial \xi} - \frac{\partial f}{\partial \xi} \frac{\partial \varphi}{\partial \eta} \right] - \frac{3}{4} f \frac{\partial \varphi}{\partial \eta} = \frac{\partial^2 \varphi}{\partial \eta^2} \quad (9.c)$$

with boundary conditions given by,

$$\left. \frac{\partial f}{\partial \eta} \right|_{\eta=0} = \frac{u_f(\xi, \delta) \xi^{-1/2}}{D_{vg} \zeta^2} \quad (9.d)$$

$$f(\xi, 0) = \frac{4}{3} \frac{\dot{m}^* \xi^{1/4}}{\rho D_{vg} \zeta} - \frac{4}{3} \xi \left. \frac{\partial f}{\partial \xi} \right|_{\eta=0} \quad (9.e)$$

$$\left. \frac{\partial f}{\partial \eta} \right|_{\eta \rightarrow \infty} = 0 \quad (9.f)$$

$$\theta(\xi, 0) = \frac{T_i - T_\infty}{T_w - T_\infty}; \quad \theta(\xi, \eta \rightarrow \infty) = 0 \quad (9.g,h)$$

$$\frac{\dot{m}^* \xi^{1/4}}{\rho D_{vg} \zeta} \varphi(\xi, 0) + \left. \frac{\partial \varphi}{\partial \eta} \right|_{\eta=0} = - \frac{\dot{m}^* \xi^{1/4}}{\rho D_{vg} \zeta} W_\infty \quad (9.i)$$

$$\varphi(\xi, \eta \rightarrow \infty) = 0 \quad (9.j)$$

where Sc and Pr are the Schmidt and Prandtl numbers for the gas mixture. It is also important to mention that, even though eqs. (9.f,h,j) impose boundary conditions at infinity, from a computational point-of-view, they are imposed at a finite η ; more specifically, at $\eta = \eta_f$.

2.4.2. Implicit filter

Decomposing the dependent variables in filter and filtered functions may be used to homogenize the equations and boundary conditions source terms, with an associated benefit in convergence behavior [20]. Among possible filtering schemes, the implicit filter allows the user to choose boundary conditions for the filtered potentials, at the expense of having to solve unknown terms together with the transformed problem [42,43]. Given the complex nature of the boundary conditions of eqs. (9. e,g,i), an implicit filter is used and the dependent variables are decomposed as,

$$f(\xi, \eta) = F(\xi, \eta) + f^*(\xi, \eta) \quad (10.a)$$

$$\theta(\xi, \eta) = \theta_F(\xi, \eta) + \theta^*(\xi, \eta) \quad (10.b)$$

$$\varphi(\xi, \eta) = \varphi_F(\xi, \eta) + \varphi^*(\xi, \eta) \quad (10.c)$$

In addition, the following boundary conditions are chosen for the filtered potentials:

$$\left. \frac{\partial f^*}{\partial \eta} \right|_{\eta=0} = 0; \quad f^*(\xi, 0) = 0 \quad (11.a,b)$$

$$\left. \frac{\partial f^*}{\partial \eta} \right|_{\eta=\eta_f} = 0 \quad (11.c)$$

$$\theta^*(\xi, 0) = 0; \quad \theta^*(\xi, \eta_f) = 0 \quad (11.d,e)$$

$$\varphi^*(\xi, 0) = 0; \quad \varphi^*(\xi, \eta_f) = 0 \quad (11.f,g)$$

Substituting eqs. (10.a-c) and (11.a-g) into the boundary conditions of eqs. (9.d-j) and proposing quadratic, for $F(\xi, \eta)$, and linear, for $\theta_F(\xi, \eta)$

and $\varphi_F(\xi, \eta)$, polynomials in η , yields

$$F(\xi, \eta) = a_0(\xi) + \frac{u_f(\xi, \delta) \xi^{-1/2}}{D_{vg} \zeta^2} \eta \left(1 - \frac{\eta}{\eta_f} \right) \quad (12.a)$$

$$\theta_F(\xi, \eta) = \frac{T_i - T_\infty}{T_w - T_\infty} \left(1 - \frac{\eta}{\eta_f} \right) \quad (12.b)$$

$$\varphi_F(\xi, \eta) = c_0(\xi) \left(1 - \frac{\eta}{\eta_f} \right) \quad (12.c)$$

where the unknown coefficients are determined from the following equations:

$$\xi \frac{da_0}{d\xi} + \frac{3}{4} a_0(\xi) = \frac{\dot{m}^* \xi^{1/4}}{\rho D_{vg} \zeta} - \xi \left. \frac{\partial f^*}{\partial \xi} \right|_{\eta=0} \quad (12.d)$$

$$c_0(\xi) \left(\frac{\dot{m}^* \xi^{1/4}}{\rho D_{vg} \zeta} - \frac{1}{\eta_f} \right) = - \frac{\dot{m}^* \xi^{1/4}}{\rho D_{vg} \zeta} W_\infty - \left. \frac{\partial \varphi^*}{\partial \eta} \right|_{\eta=0} \quad (12.e)$$

Upon employing the decompositions of eqs. (10.a-c) into eqs. (9.a-c), one then arrives at,

$$\begin{aligned} \xi \left[\frac{\partial f^*}{\partial \eta} \frac{\partial^2 f^*}{\partial \xi \partial \eta} - \frac{\partial^2 f^*}{\partial \eta^2} \frac{\partial f^*}{\partial \xi} + \frac{\partial F}{\partial \eta} \frac{\partial^2 f^*}{\partial \xi \partial \eta} - \frac{\partial^2 F}{\partial \eta^2} \frac{\partial f^*}{\partial \xi} + \frac{\partial f^*}{\partial \eta} \frac{\partial^2 F}{\partial \xi \partial \eta} - \frac{\partial^2 f^*}{\partial \eta^2} \frac{\partial F}{\partial \xi} \right] \\ + \frac{1}{2} \left(\frac{\partial f^*}{\partial \eta} \right)^2 - \frac{3}{4} \left[f^* \frac{\partial^2 f^*}{\partial \eta^2} + F \frac{\partial^2 f^*}{\partial \eta^2} + f^* \frac{\partial^2 F}{\partial \eta^2} \right] + \frac{\partial F}{\partial \eta} \frac{\partial f^*}{\partial \eta} \\ = Sc \frac{\partial^3 f^*}{\partial \eta^3} + Sc[\varphi_F + \varphi^*] + Sc \frac{\beta_T}{\beta_c} (T_\infty - T_w)[\theta_F + \theta^*] + \frac{3}{4} F \frac{\partial^2 F}{\partial \eta^2} - \frac{1}{2} \left(\frac{\partial F}{\partial \eta} \right)^2 \\ - \xi \left[\frac{\partial F}{\partial \eta} \frac{\partial^2 F}{\partial \xi \partial \eta} - \frac{\partial F}{\partial \xi} \frac{\partial^2 F}{\partial \eta^2} \right] \end{aligned} \quad (13.a)$$

$$\begin{aligned} \xi \left[\frac{\partial f^*}{\partial \eta} \frac{\partial \theta^*}{\partial \xi} - \frac{\partial f^*}{\partial \xi} \frac{\partial \theta^*}{\partial \eta} + \frac{\partial F}{\partial \eta} \frac{\partial \theta^*}{\partial \xi} - \frac{\partial F}{\partial \xi} \frac{\partial \theta^*}{\partial \eta} + \frac{\partial f^*}{\partial \eta} \frac{\partial \theta_F}{\partial \xi} - \frac{\partial f^*}{\partial \xi} \frac{\partial \theta_F}{\partial \eta} \right] \\ - \frac{3}{4} \left[f^* \frac{\partial \theta^*}{\partial \eta} + F \frac{\partial \theta^*}{\partial \eta} + f^* \frac{\partial \theta_F}{\partial \eta} \right] = \frac{Sc}{Pr} \frac{\partial^2 \theta^*}{\partial \eta^2} + \frac{3}{4} F \frac{\partial \theta_F}{\partial \eta} \\ - \xi \left[\frac{\partial F}{\partial \eta} \frac{\partial \theta_F}{\partial \xi} - \frac{\partial F}{\partial \xi} \frac{\partial \theta_F}{\partial \eta} \right] \end{aligned} \quad (13.b)$$

$$\begin{aligned} \xi \left[\frac{\partial f^*}{\partial \eta} \frac{\partial \varphi^*}{\partial \xi} - \frac{\partial f^*}{\partial \xi} \frac{\partial \varphi^*}{\partial \eta} + \frac{\partial F}{\partial \eta} \frac{\partial \varphi^*}{\partial \xi} - \frac{\partial F}{\partial \xi} \frac{\partial \varphi^*}{\partial \eta} + \frac{\partial f^*}{\partial \eta} \frac{\partial \varphi_F}{\partial \xi} - \frac{\partial f^*}{\partial \xi} \frac{\partial \varphi_F}{\partial \eta} \right] \\ - \frac{3}{4} \left[f^* \frac{\partial \varphi^*}{\partial \eta} + F \frac{\partial \varphi^*}{\partial \eta} + f^* \frac{\partial \varphi_F}{\partial \eta} \right] = \frac{\partial^2 \varphi^*}{\partial \eta^2} + \frac{3}{4} F \frac{\partial \varphi_F}{\partial \eta} \\ - \xi \left[\frac{\partial F}{\partial \eta} \frac{\partial \varphi_F}{\partial \xi} - \frac{\partial F}{\partial \xi} \frac{\partial \varphi_F}{\partial \eta} \right] \end{aligned} \quad (13.c)$$

2.4.3. Eigenvalue problems

To proceed with the integral transform process, eigenvalue problems must be proposed for each dependent variable. The chosen homogeneous boundary conditions of eqs. (11.a-g) are also imposed onto the eigenvalue problems. For the filtered dimensionless streamfunction, f^* , a third order eigenvalue problem is used, based on the following ordinary differential equation:

$$\frac{d^3 \psi_{f,m}}{d\eta^3} + \lambda_{f,m}^2 \psi_{f,m}(\eta) = 0, \quad m = 1, 2, 3, \dots \quad (14.a)$$

with boundary conditions and normalization given by,

$$\psi_{f,m}(0) = 0; \quad \psi'_{f,m}(0) = 0 \quad (14.b,c)$$

$$\psi'_{f,m}(\eta_f) = 0 \quad (14.d)$$

$$N_{f,m} = \int_0^{\eta_f} \psi'_{f,m}(\eta)^2 d\eta; \quad \tilde{\psi}_{f,m}(\eta) = \frac{\psi_{f,m}(\eta)}{\sqrt{N_{f,m}}} \quad (14.e,f)$$

and bearing the following orthogonality property,

$$\int_0^{\eta_f} \tilde{\psi}_{f,m}(\eta) \tilde{\psi}_{f,n}(\eta) d\eta = \delta_{mn} \quad (14.g)$$

where $\psi_{f,m}$ and $\lambda_{f,m}$ are the eigenfunction and associated eigenvalue for the dimensionless streamfunction, respectively, and δ_{mn} is Kronecker's delta.

For the filtered dimensionless temperature and mass fraction, a second order eigenproblem is proposed, based on the following one-dimensional Helmholtz equation:

$$\frac{d^2 \psi_{\theta\varphi,m}}{d\eta^2} + \lambda_{\theta\varphi,m}^2 \psi_{\theta\varphi,m}(\eta) = 0, m = 1, 2, 3, \dots \quad (15.a)$$

with boundary conditions and normalization given by,

$$\psi_{\theta\varphi,m}(0) = 0; \quad \psi_{\theta\varphi,m}(\eta_f) = 0 \quad (15.b,c)$$

$$N_{\theta\varphi,m} = \int_0^{\eta_f} \psi_{\theta\varphi,m}(\eta) \psi_{\theta\varphi,m}(\eta) d\eta; \quad \tilde{\psi}_{\theta\varphi,m}(\eta) = \frac{\psi_{\theta\varphi,m}(\eta)}{\sqrt{N_{\theta\varphi,m}}} \quad (15.d,e)$$

and bearing the following orthogonality property,

$$\int_0^{\eta_f} \tilde{\psi}_{\theta\varphi,m}(\eta) \tilde{\psi}_{\theta\varphi,n}(\eta) d\eta = \delta_{mn} \quad (15.f)$$

where $\psi_{\theta\varphi,m}$ and $\lambda_{\theta\varphi,m}$ are the eigenfunction and associated eigenvalue for the dimensionless temperature and mass fraction, respectively.

2.4.4. Transformed problems

The orthogonality properties of eqs. (14.g) and (15.f) allow for the establishment of the following transform-inverse pairs:

Transforms:

$$\bar{f}_m(\xi) = \int_0^{\eta_f} \tilde{\psi}_{f,m}(\eta) f^*(\xi, \eta) d\eta \quad (16.a)$$

$$\bar{\theta}_m(\xi) = \int_0^{\eta_f} \tilde{\psi}_{\theta\varphi,m}(\eta) \theta^*(\xi, \eta) d\eta \quad (16.b)$$

$$\bar{\varphi}_m(\xi) = \int_0^{\eta_f} \tilde{\psi}_{\theta\varphi,m}(\eta) \varphi^*(\xi, \eta) d\eta \quad (16.c)$$

Inverses:

$$f^*(\xi, \eta) = \sum_{m=1}^{\infty} \bar{f}_m(\xi) \tilde{\psi}_{f,m}(\eta) \quad (16.d)$$

$$\theta^*(\xi, \eta) = \sum_{m=1}^{\infty} \bar{\theta}_m(\xi) \tilde{\psi}_{\theta\varphi,m}(\eta) \quad (16.e)$$

$$\varphi^*(\xi, \eta) = \sum_{m=1}^{\infty} \bar{\varphi}_m(\xi) \tilde{\psi}_{\theta\varphi,m}(\eta) \quad (16.f)$$

Applying $\int_0^{\eta_f} \tilde{\psi}_{f,m}(\eta) (\cdot) d\eta$ to eqs. (13.a) and $\int_0^{\eta_f} \tilde{\psi}_{\theta\varphi,m}(\eta) (\cdot) d\eta$ to eqs.

(13.b,c), reuniting with eqs. (5), (6), and (12.d,e), substituting the

inverse formulae of eqs. (16.d-f), and rearranging, yields,

$$\sum_{q=1}^{\infty} \sum_{n=1}^{\infty} \left\{ A_{mnq} \xi \bar{f}_n \frac{d\bar{f}_q}{d\xi} + \frac{1}{2} \left(A_{1,mnq} + \frac{3}{2} A_{2,mnq} \right) \bar{f}_n \bar{f}_q \right\} + Sc \lambda_{f,m}^2 \bar{f}_m + \sum_{n=1}^{\infty} \left\{ B_{mn} \xi \frac{d\bar{f}_n}{d\xi} + C_{mn} \bar{f}_n \right\} = Sc \bar{\varphi}_m + Sc \frac{\beta_T}{\beta_c} (T_{\infty} - T_w) \bar{\theta}_m + \bar{g}_{f,m} \quad (17.a)$$

$$\sum_{q=1}^{\infty} \sum_{n=1}^{\infty} \left\{ D_{mnq} \xi \bar{f}_n \frac{d\bar{\theta}_q}{d\xi} + E_{mnq} \xi \frac{d\bar{f}_n}{d\xi} \bar{\theta}_q + \frac{3}{4} E_{mnq} \bar{f}_n \bar{\theta}_q \right\} + \frac{Sc}{Pr} \lambda_{\theta\varphi,m}^2 \bar{\theta}_m + \sum_{n=1}^{\infty} \left\{ G_{mn} \xi \frac{d\bar{\theta}_n}{d\xi} + H_{mn} \bar{\theta}_n + K_{mn} \xi \frac{d\bar{f}_n}{d\xi} + L_{mn} \bar{f}_n \right\} = \bar{g}_{\theta,m} \quad (17.b)$$

$$\sum_{q=1}^{\infty} \sum_{n=1}^{\infty} \left\{ D_{mnq} \xi \bar{f}_n \frac{d\bar{\varphi}_q}{d\xi} + E_{mnq} \xi \frac{d\bar{f}_n}{d\xi} \bar{\varphi}_q + \frac{3}{4} E_{mnq} \bar{f}_n \bar{\varphi}_q \right\} + \lambda_{\theta\varphi,m}^2 \bar{\varphi}_m + \sum_{n=1}^{\infty} \left\{ G_{mn} \xi \frac{d\bar{\varphi}_n}{d\xi} + H_{mn} \bar{\varphi}_n + O_{mn} \xi \frac{d\bar{f}_n}{d\xi} + P_{mn} \bar{f}_n \right\} = \bar{g}_{\varphi,m} \quad (17.c)$$

$$\frac{d(\delta^4)}{d\xi} = \frac{4L_l^2}{g} c_{p,l} (T_{\infty} - T_w) \left\{ \frac{T_i - T_w}{T_{\infty} - T_w} + \frac{T_i - T_{\infty}}{T_{\infty} - T_w} \frac{k}{k_l} \frac{\delta}{\xi^{1/4}} \frac{\zeta}{\eta_f} + \frac{k}{k_l} \zeta \frac{\delta}{\xi^{1/4}} \sum_{m=1}^{\infty} \tilde{\psi}_{\theta\varphi,m}(0) \bar{\theta}_m \right\} \quad (17.d)$$

$$\xi \frac{da_0}{d\xi} + \frac{3}{4} a_0(\xi) = \frac{\dot{m}^* \xi^{1/4}}{\rho D_{vg} \zeta} - \xi \sum_{m=1}^{\infty} \tilde{\psi}_{f,m}(0) \frac{d\bar{f}_m}{d\xi} \quad (17.e)$$

$$c_0(\xi) \left(\frac{\dot{m}^* \xi^{1/4}}{\rho D_{vg} \zeta} - \frac{1}{\eta_f} \right) = - \frac{\dot{m}^* \xi^{1/4}}{\rho D_{vg} \zeta} W_{\infty} - \sum_{m=1}^{\infty} \tilde{\psi}_{\theta\varphi,m}(0) \bar{\varphi}_m \quad (17.f)$$

with an initial condition for the liquid film thickness given by,

$$\delta(0) = 0 \quad (17.g)$$

where Pr_l and $c_{p,l}$ are the Prandtl number and the specific heat at constant pressure of the liquid, respectively. Expressions for the integral coefficients are provided in Appendix A.

2.5. Computational procedure

From a computational standpoint, it is impossible to solve the infinitely large coupled ordinary differential equations system of eqs. (17.a-f); thus, truncation to finite orders is inevitable. The inverse formulae of eqs. (16.d,e,f) are hence truncated to finite orders \mathcal{N}_f , \mathcal{N}_{θ} , \mathcal{N}_{φ} , respectively. These truncation orders then trickle down to the ordinary differential equations systems of eqs. (17.a-f), thereby leading to a finite system of equations, and are the only parameters to monitor for checking the convergence of the results.

Analytical expressions for the integral coefficients of eqs. (A.1.a-p) are obtained with symbolic computation using the *Wolfram Mathematica v.12.3* platform [44]. The numerical values of these coefficients are then attained with binaries programmed in C++ running in the GPU (Graphics Processing Unit) and using functions built-in the *Mathematica* environment to feed and retrieve data from the video memory.

When $x \rightarrow 0$, $\eta \rightarrow \infty$; thus, the boundary conditions at $\xi = x = 0$ of eqs. (4.e-g) are already conveyed by the boundary conditions of eqs. (9.f,h,j). Any conditions imposed at $\xi \rightarrow 0$ are expected to be short-lived and confined to an infinitely small portion adjacent to the liquid film. Nonetheless, the numerical integration algorithm still needs starting values. For simplicity, the filters are used as initial conditions, yielding the following initial conditions:

$$a_0(\xi \rightarrow 0) = 0; \quad \left. \frac{\partial f^*}{\partial \eta} \right|_{\xi \rightarrow 0} = 0 \quad (18.a,b)$$

$$\theta^*(\xi \rightarrow 0, \eta) = 0; \quad \varphi^*(\xi \rightarrow 0, \eta) = 0 \quad (18.c,d)$$

To avoid the singularities of eqs. (17.a-f) at $\xi = 0$, their integration is started at a small but finite value, for instance, $\xi = 10^{-6}$. Moreover, instead of strictly imposing eq. (17.g) and dealing with the associated singularity it introduces into eq. (17.d), an approximate value, δ_0 , calculated at $\xi = x = 10^{-6}$ m with the classical Nusselt model for the film thickness (see eq. B.1.a), is imposed as initial condition for δ . Similarly, the right-hand sides of eqs. (18.a-d) are set to a small finite value, i.e., 10^{-6} . More detailed initial conditions are provided in Appendix B.

The numerical integration of the transformed problem of eqs. (17.a-g) is carried out with the Implicit Differential-Algebraic (IDA) method [45] built-in the function *NDSolve* from *Wolfram Mathematica v.12.3* [44]. At least 8-digit accuracy and precision goals are set for error control in *NDSolve*'s algorithm. Once the transformed potentials \bar{f}_m , $\bar{\theta}_m$, and $\bar{\varphi}_m$ are numerically calculated, the inverse formulae, eqs. (16.d-f), and the filtering decompositions, eqs. (10.a-c), can be used to recover the dimensionless streamfunction, temperature, and mass fraction.

The results of this work are obtained for a gas mixture consisting of water vapor and air. The thermophysical properties for liquid water and for the humid air are obtained from tables and correlations available in the literature [46,47] using the film temperature $0.5(T_w + T_\infty)$. The exception is the thermal expansion coefficient, which is evaluated at the bulk temperature, T_∞ . Each simulation run takes at most 14 min in an Intel i7 11800H, 64 GB DDR4, NVIDIA RTX 3050 computer for $\mathcal{N}_f = 100$, $\mathcal{N}_\theta = 100$, and $\mathcal{N}_\varphi = 200$, and accuracy and precision goals set to 8 digits in the *NDSolve* routine.

2.6. Post-processing

Several quantities derived from already defined variables are used to present and analyze the results attained with the described solution procedure. To ease the understanding of the results, the definitions used for these quantities are provided in this section.

The heat flux at the wall can be determined with Fourier's law applied to the liquid film as follows,

$$q_w = k_l \frac{T_i - T_w}{\delta} \quad (19)$$

where q_w is the local heat flux at the wall.

Defining the local heat transfer coefficient as,

$$h = \frac{q_w}{T_\infty - T_w} = \frac{k_l}{\delta} \frac{T_i - T_w}{T_\infty - T_w} \quad (20.a)$$

one then obtains,

$$h_m = \frac{1}{L} \int_0^L h dx \quad (20.b)$$

$$Nu_m = \frac{h_m L}{k} \quad (20.c)$$

where h_m and Nu_m are the average heat transfer coefficient and Nusselt number, respectively.

The heat transfer rate per unit of depth can be obtained through integration of eq. (19), yielding,

$$\dot{Q}' = \int_0^L q_w dx \quad (21)$$

where \dot{Q}' is the heat transfer rate per unit of depth and L is the height of the vertical wall depicted in Fig. 1.

A comparative metric against results from the classical Nusselt model for pure vapor film condensation [38] will be useful further in the text.

More specifically, it is defined as the ratio between the heat transfer per unit of depth obtained from eq. (21), \dot{Q}' , and the one calculated according to the Nusselt model, \dot{Q}'_{Nu} , which can be calculated as [14,38],

$$\dot{Q}'_{Nu} = \frac{4}{3} \mu_l h_{fg} \left[\frac{c_{p,l}(T_\infty - T_w)}{Pr_l h_{fg}} \right]^{3/4} \left(\frac{g L^3}{4\nu_l^2} \right)^{1/4} \quad (22)$$

where \dot{Q}'_{Nu} is the heat transfer rate per unit of depth for pure saturated vapor film condensation.

3. Results and discussion

3.1. Convergence analysis

Table 1 presents the convergence behavior of the gas mixture velocity at the interface and the ratio \dot{Q}'/\dot{Q}'_{Nu} with varying truncation orders \mathcal{N}_f , \mathcal{N}_θ , and \mathcal{N}_φ . For the velocity, values at four different vertical positions are shown. The numerical values are attained with a bulk mass fraction of 0.1, a wall height of 0.1 m, a total pressure of 1 atm, and a degree of subcooling of 30 °C. The convergence of both the velocity at the interface and the ratio of heat transfer rates are deemed satisfactory, with the highest employed truncation order achieving at least three significant fully converged digits.

The last four lines in Table 1 serve the purpose of probing the relative importance of each truncation order. From the changes in the values observed with the subtraction of 10 terms from each order we can assert that the results are more sensitive to the truncation order of the mass fraction, \mathcal{N}_φ , by noting that, percentagewise, it suffered the lowest change while still affecting the velocity and heat transfer at least as much as going from $\mathcal{N}_f = 100$ to $\mathcal{N}_f = 90$ does. For this reason, \mathcal{N}_φ must assume values considerably larger than \mathcal{N}_f and \mathcal{N}_θ to achieve a satisfactorily converged result, while keeping the computational cost as low as possible. Henceforth, 100, 100, and 200 are respectively adopted as the truncation orders \mathcal{N}_f , \mathcal{N}_θ , and \mathcal{N}_φ .

3.2. Experimental validation

Fig. 2 shows a comparison between results of the present work and measurements of heat transfer rates for condensation on vertical walls in the presence of a non-condensable gas [13]. Six graphs are displayed, each containing results for a different bulk mass fraction, W_∞ . In all of them, the ratio of heat transfer rates, \dot{Q}'/\dot{Q}'_{Nu} , is plotted as a function of the subcooling, as given by the temperature difference $T_\infty - T_w$. As can be seen from the data, the agreement is overall good. Yet, larger deviations are observed for the two lowest bulk mass fractions. A clue to the reason can be found in the experimental work [13], which posits that the experimental uncertainties are expected to be large for low W_∞ due to the difficulty in measuring this quantity accurately and the high sensitivity of the heat transfer rate even to small deviations in the bulk

Table 1
Convergence analysis of the heat transfer rate, and the interfacial velocity with varying truncation orders. Entry data: $W_\infty = 0.1$; $L = 0.1$ m; $T_\infty - T_w = 30$ °C; $p = 1$ atm; $\eta_f = 6.8$.

\mathcal{N}_f	\mathcal{N}_θ	\mathcal{N}_φ	$u(x, \delta)$ (mm/s)				$\frac{\dot{Q}'}{\dot{Q}'_{Nu}}$
			$x = 20$ mm	$x = 40$ mm	$x = 60$ mm	$x = 80$ mm	
60	60	160	18.175	25.682	31.444	36.304	0.13132
70	70	170	18.182	25.684	31.440	36.293	0.13124
80	80	180	18.201	25.713	31.476	36.335	0.13147
90	90	190	18.213	25.730	31.499	36.363	0.13164
90	100	200	18.223	25.742	31.512	36.376	0.13170
100	90	200	18.229	25.760	31.541	36.417	0.13196
100	100	190	18.212	25.727	31.493	36.353	0.13158
100	100	200	18.228	25.759	31.540	36.415	0.13195

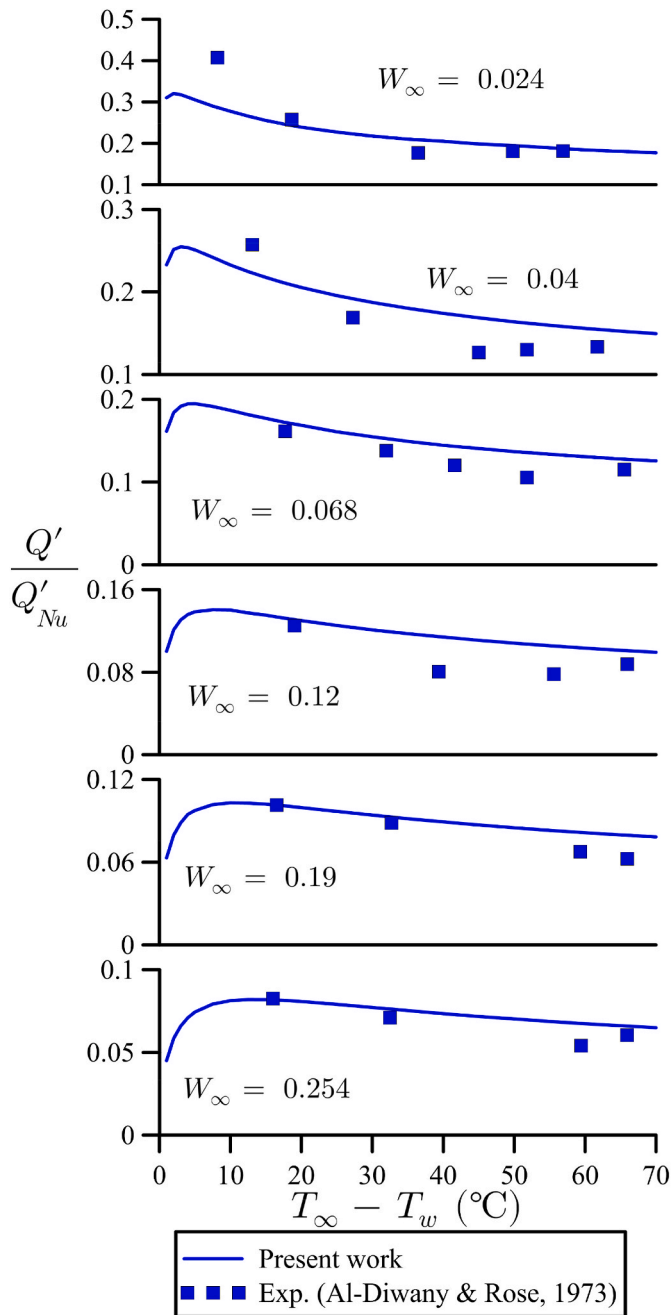


Fig. 2. Validation of the method and computational code against experimental results. Q'/Q'_{Nu} as a function of the degree of subcooling, $T_\infty - T_w$, for six different bulk mass fractions.

mass fraction. Moreover, the ratio of heat transfer is considerably lower than one for all cases illustrated in Fig. 2, thereby providing further confirmation of the dramatic effect that fairly small amounts of non-condensing gases can have on heat transfer performance.

Fig. 3 depicts the heat transfer ratio as a function of the bulk mass fraction. Solid lines stand for results from the proposed methodology and computational code; three curves are provided, each for a different degree of subcooling. Symbols stem from experimental results for degrees of subcooling above and below 20 °C [13]. As observed, once more, the results from the present work compare favorably with the experimental ones, further confirming the adequacy of the proposed methodology. In the lower range of mass fractions, the deviation between hybrid numerical-analytical results and experimental data is larger for the reasons already discussed in the context of Fig. 2.

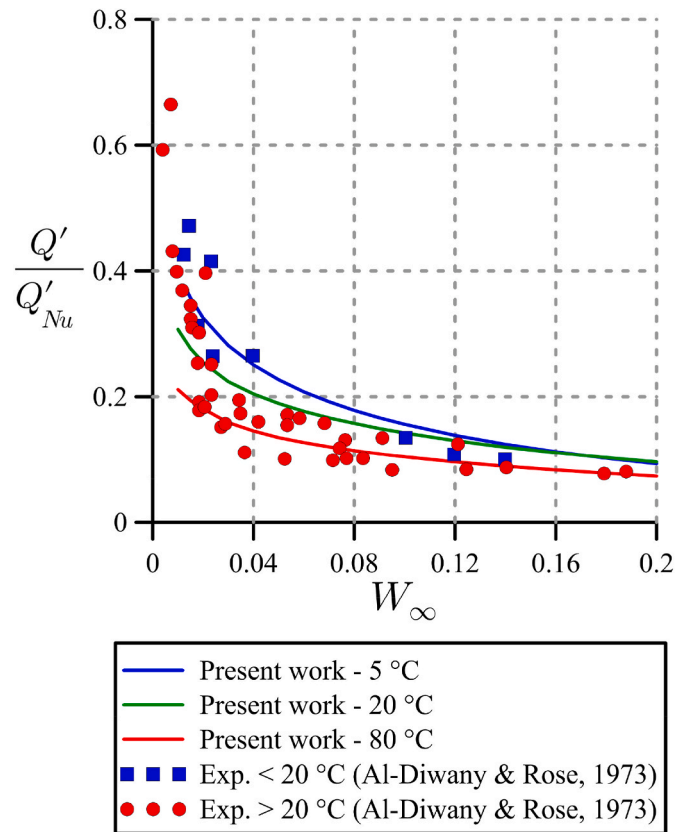


Fig. 3. Validation of the method and computational code against experimental results. Q'/Q'_{Nu} as a function of bulk mass fraction obtained numerically and experimentally for three and two degrees of subcooling, respectively.

3.3. Comparison with Karman-Pohlhausen's integral method and physical analysis

Four parameters were identified as being capable of conveying all physical information contained within the present model, namely the absolute total pressure p , the bulk mass fraction W_∞ , the concentration Rayleigh number $Ra_c \equiv g\beta_c L^3 / \nu D_{vg}$, and the Jakob number $Ja \equiv c_{p,l}(T_\infty - T_w) / h_{fg}$. Even the film temperature, which serves to determine the values of the thermophysical properties, can be uniquely determined from the knowledge of W_∞ and Ja . Thus, for the sake of conciseness, we shall restrict the analysis to varying dimensionless parameters W_∞ , Ra_c , and Ja , while keeping the total pressure, p , equal to 1 atm.

A solution using the Karman-Pohlhausen integral method of a simplified version of the condensation problem in the presence of a non-condensable gas was recently reported [48]. Fig. 4a,b compare the results for the profiles of the vertical velocity component and the mass fraction in the gas mixture, respectively, from the GITT solution presented in this work with the ones from the integral method. In these graphs, velocity and mass fraction profiles are presented for three different values of bulk mass fraction, W_∞ , while setting $Ra_c = 10^6$, and $Ja = 0.05$. A logarithmic scale is employed in the horizontal axis of the graphs to highlight the near-condensate-film region, since the involved transport phenomena between the gas mixture and the liquid film are mostly governed by what happens in this portion of the gas mixture. Inasmuch as the integral method is not intended to fully capture the information of the profiles along y [41], it is still capable of producing fairly good results near the condensate film. Deviations between the GITT and the integral method results are larger for the velocity than for the mass fraction, due to the approximate manner the latter treats the profiles along y [41]. Nonetheless, the comparison provides further

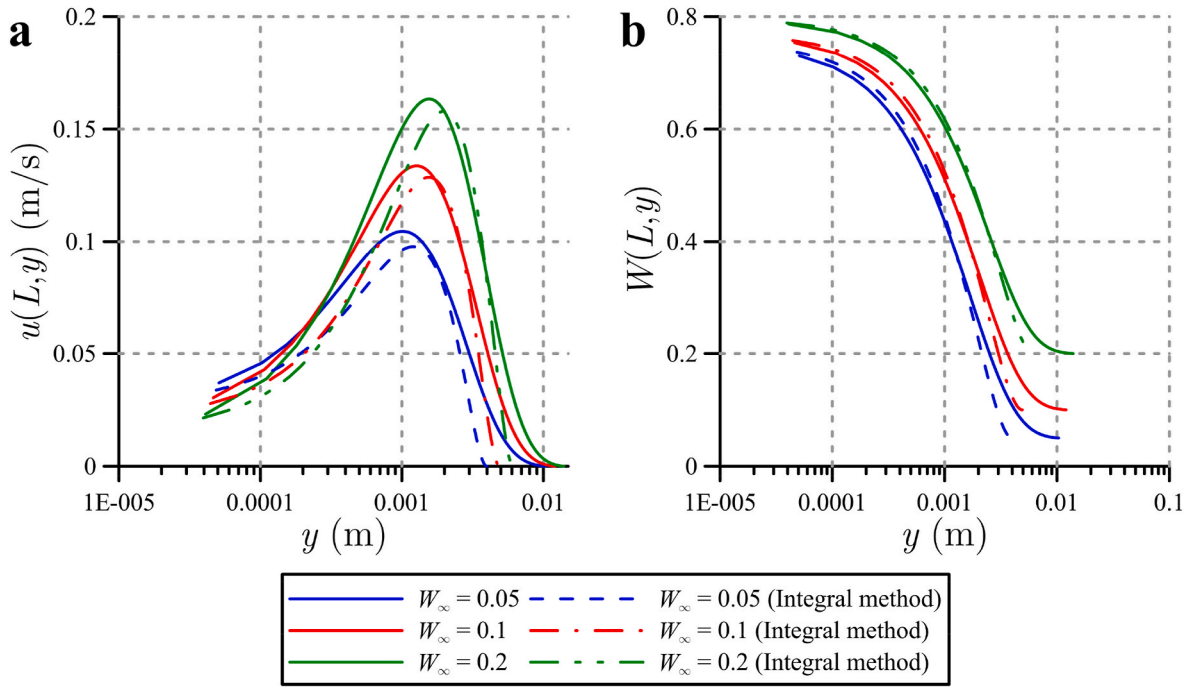


Fig. 4. Comparison of the GITT with results from the integral method with varying bulk mass fraction. Values for the remaining entry parameters are $Ra_c = 10^6$, and $Ja = 0.05$. (a) Vertical velocity component profile in the gas mixture at the bottom of the wall depicted in Fig. 1; (b) Mass fraction profile in the gas mixture at the bottom of the wall depicted in Fig. 1.

verification of the proposed solution methodology against results from a completely independent approach to deal with the boundary layers involved in the condensation process.

The lower velocities and higher non-condensable gas mass fractions at the interface between the liquid film and the gas mixture with rising bulk mass fractions of non-condensing substance is a sign of the detrimental effects it has on the condensation process. With less condensate

output, the drag imposed by the liquid film is smaller, rendering lower gas mixture velocities near the interface. As for the mass fraction of non-condensable gas at the interface, it grows with higher bulk mass fractions, thus indicating a more severe accumulation of this substance at this location, precluding the vapor from reaching the condensing site.

Further verification of the solution methodology proposed in this work is provided by the velocity and mass fraction profiles of Fig. 5a,b

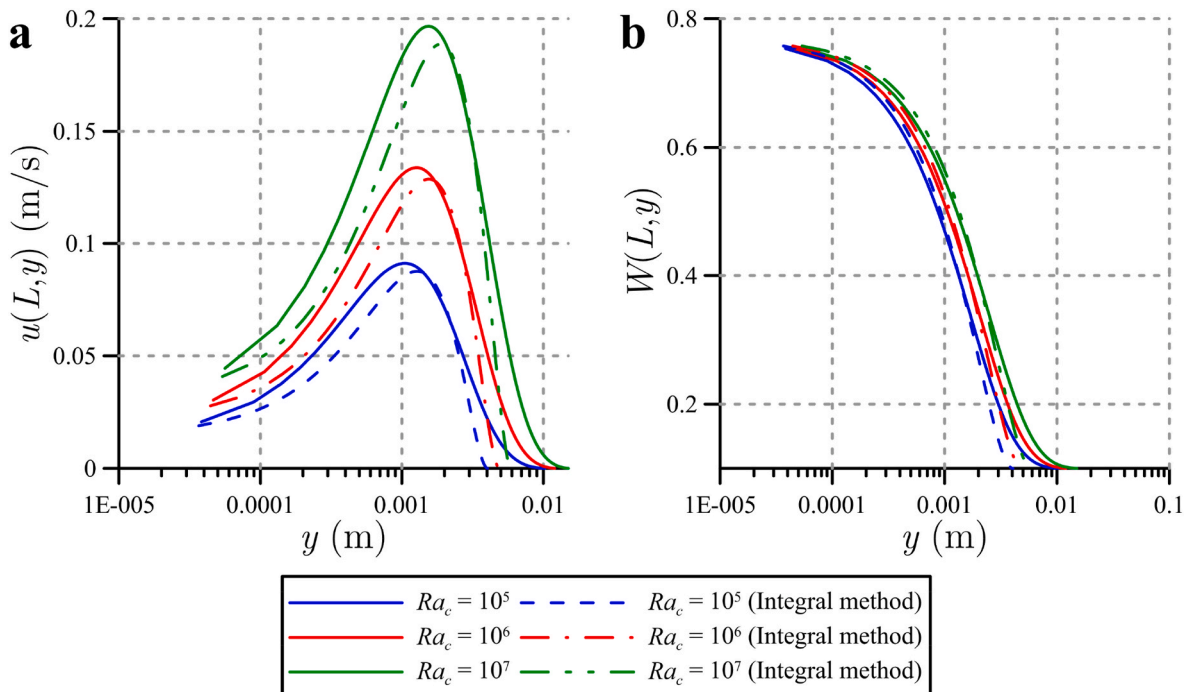


Fig. 5. Comparison of the GITT with results from the integral method with varying concentration Rayleigh number. Values for the remaining entry parameters are $W_\infty = 0.1$, and $Ja = 0.05$. (a) Vertical velocity component profile in the gas mixture at the bottom of the wall depicted in Fig. 1; (b) Mass fraction profile in the gas mixture at the bottom of the wall depicted in Fig. 1.

stemming from both the GITT and the integral method. In these graphs, Rayleigh is set to three different values spanning three orders of magnitude between 10^5 and 10^7 , while $W_\infty = 0.1$ and $Ja = 0.05$. Despite its shortcomings, the integral method results are relatively close to the GITT ones, especially for the mass fraction profiles, which adds to the verification effort of the GITT procedure against a different methodology and computational code.

Raising the concentration Rayleigh number has a substantial effect on the velocity magnitudes, indicating that natural convection is at least as important to determine the gas mixture flow as the drag force effected by the gravity-induced downward flow of the condensate film. On the other hand, the mass fraction, especially at the interface is rather insensible to changes in Ra_c .

A final verification effort is made by evaluating the velocity and mass fraction profiles for varying values of the Jakob number, as depicted in Fig. 6a,b. The pattern of marginal agreement between the velocity profiles and very good agreement between the mass fraction profiles obtained with the GITT and integral methods is repeated. As these results stem from independent solution methodologies and given the agreement found between GITT and experimental results in section 3.2, we can infer that the proposed approach is adequate to the analysis of external boundary layer flows, even when complex phenomena such as condensation in the presence of non-condensables is considered.

The Jakob number, Ja , represents the main driving force for the condensation process, i.e., it is proportional to $T_\infty - T_w$. Therefore, its effect on the mass fraction profiles of Fig. 6 a is significant and higher values of Ja are associated with higher values of non-condensable gas mass fraction at the interface. Physically, the vapor is more effectively depleted when the driving force increases, which explains the observed behavior.

The last set of results are dedicated to examining the behavior of the ratio of heat transfer rates and the average Nusselt number with the variation of the parameters Ra_c , W_∞ , and Ja . Fig. 7 a shows how the ratio of heat transfer rates, \dot{Q}/\dot{Q}'_{Nu} , and the average Nusselt number, Nu_m , behave when the concentration Rayleigh number, Ra_c , is varied. Even though the contemplated values of Ra_c span three orders of magnitude,

the change in the ratio of heat transfer rates is negligible. This indicates that the heat transfer rate per unit of depth obtained in the presence of a non-condensable gas retains the same scale with the Rayleigh number as the one in the classical Nusselt model for condensation of pure vapor, i. e., $\dot{Q} \propto Ra_c^{1/4}$ (see eq. (22)). Consequently, since the wall height, L , is present only in Ra_c , this scaling leads to the conclusion that the heat transfer rate scales with $L^{3/4}$. As for the average Nusselt number, it greatly increases with rising Ra_c , for stronger natural convection favors convective heat transfer and vapor mass transport to the interface between the gas mixture and the condensate film, thereby improving condensation heat transfer.

In Fig. 7b,c, the behavior of the ratio of heat transfer rates and the average Nusselt number are probed with varying bulk mass fraction, W_∞ , and Jakob number, Ja , respectively. Both \dot{Q}/\dot{Q}'_{Nu} and Nu_m decrease when more non-condensable gas is present, which mirrors the behavior observed in Fig. 3 and in other experimental and numerical contributions [13–15]. As previously stated, this fact is due to the accumulation of non-condensing substance at the interface, which blocks access of vapor molecules to the condensation sites, underscoring the importance of accounting for even small amounts of non-condensable gases in the analysis and design of processes and equipment involving condensation. A somewhat similar trend is observed with varying Jakob number, Ja . At first glance, this seems counterintuitive, given the direct relation between Ja and the driving force $T_\infty - T_w$ and the expected positive effect it has on the heat transfer rate. However, one must be aware that both the ratio of heat transfer rates and the average Nusselt number express heat transfer rates per unit of temperature difference (see eqs. (20.a-c), (21), and (22)); more specifically, the heat transfer rate is divided by $(T_\infty - T_w)^{3/4}$ and $T_\infty - T_w$ in the definitions of \dot{Q}/\dot{Q}'_{Nu} and Nu_m , respectively. Therefore, from Fig. 7 c, we can conclude that, when non-condensable gases are present, the heat transfer rate, \dot{Q} , is a weaker function of the Jakob number than occurs with pure vapor. A possible reason is the presence of the non-condensable gas partially offsetting the driving force by imposing that the temperature at the interface, T_i , be lower than the bulk one, T_∞ .

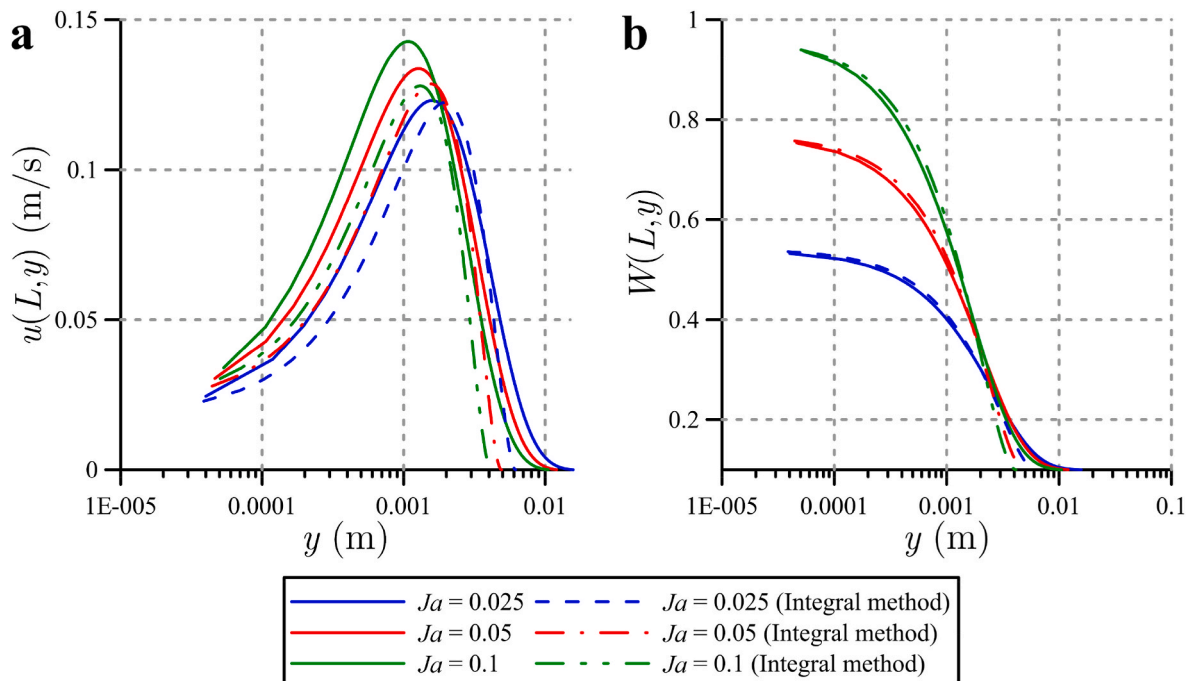


Fig. 6. Comparison of the GITT with results from the integral method with varying Jakob number. Values for the remaining entry parameters are $W_\infty = 0.1$, and $Ra_c = 10^6$. (a) Vertical velocity component profile in the gas mixture at the bottom of the wall depicted in Fig. 1; (b) Mass fraction profile in the gas mixture at the bottom of the wall depicted in Fig. 1.

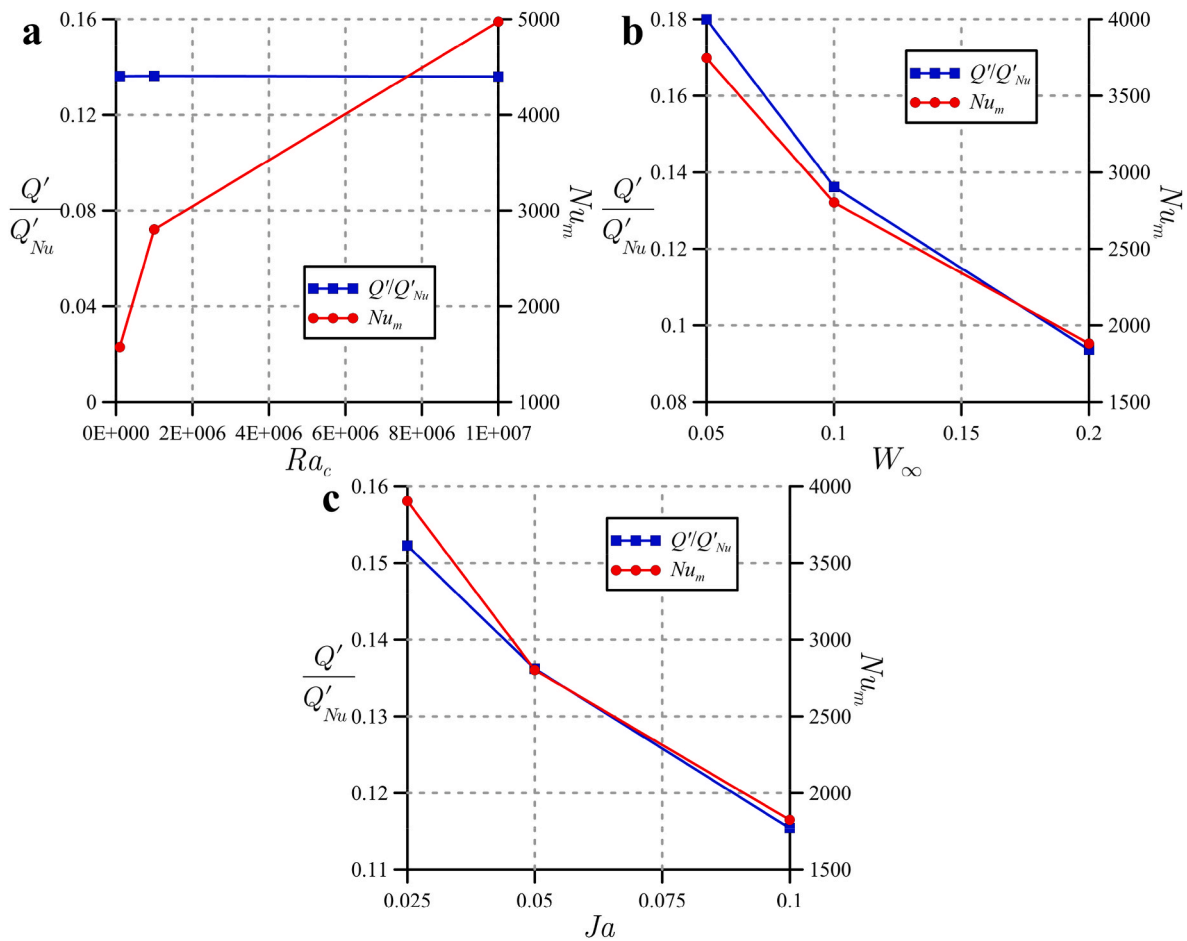


Fig. 7. Effect of concentration Rayleigh number, bulk mass fraction, and Jakob number on the ratio of heat transfer rates and the average Nusselt number. (a) Varying concentration Rayleigh number; (b) Varying bulk mass fraction; (c) Varying Jakob number. Left- and rightmost vertical axes represent \dot{Q}/\dot{Q}_{Nu} and Nu_m , respectively.

4. Conclusions

Film condensation in the presence of a non-condensable gas is theoretically analyzed. A solution methodology for external boundary layers based on the Generalized Integral Transform Technique (GITT) was proposed for this purpose. A pre-processing step to employ a physically inspired change of variables was proposed to improve manageability of the model during the integral transformation process. Similar changes of variables stemming from scale analysis are possible for all boundary layer flows [41] and can be reproduced in other applications, though the definitions of the new variables may vary to some extent from the ones herein presented.

Experimental results for condensation of water vapor in moist air on a vertical wall were used to validate the model, solution methodology, and the developed computational implementation. Moreover, comparisons with Karman-Pohlhausen's solution procedure were introduced to provide further evidence on the suitability of the proposed solution framework. Overall, the GITT proved to be capable of dealing effectively with external boundary layer flows, even when the models are complicated enough to be troublesome for purely numerical alternatives, such as finite volumes [5,17].

Finally, a brief physical analysis confirmed the dramatic effect small quantities of non-condensable gas can have on condensation heat transfer already noted in previous contributions [11,13–16]. The movement of the gas mixture, at least for the analyzed conditions, was equivalently driven by the gravity-induced downward flow of the condensate film and natural convection. In spite of the presence of the

non-condensable gas, the heat transfer rate retains the scaling with the Rayleigh number predicted by the classical Nusselt model [14,38], which means $\dot{Q} \propto L^{3/4}$. On the other hand, due to the presence of non-condensables, the temperature difference along the liquid film will necessarily be lower than the difference between the bulk temperature of the gas mixture and the wall temperature. This phenomenon is directly related to the local accumulation of non-condensable gas at the interface with the liquid film and the associated decrease in vapor pressure at this location, thereby leading to lower heat transfer rates than the ones attainable with pure vapor.

Declaration of competing interest

The authors declare that they have no known competing financial interests or personal relationships that could have appeared to influence the work reported in this paper.

Data availability

Data will be made available on request.

Acknowledgements

The authors are grateful for the financial support offered by the Brazilian Government agencies CNPq, CAPES (PROCAD/DEFESA), and FAPERJ (Grant no. E-26/010/002590/2019, E-26/211.519/2021, and E-26/200.212/2023).

APPENDIX A. INTEGRAL COEFFICIENTS

The integral coefficients present in eqs. (17.a-c) are given by,

$$A_{1,mnq} = \int_0^{\eta_f} \tilde{\psi}'_{f,m}(\eta) \tilde{\psi}'_{f,n}(\eta) \tilde{\psi}'_{f,q}(\eta) d\eta \quad (\text{A.1.a})$$

$$A_{2,mnq} = - \int_0^{\eta_f} \tilde{\psi}'_{f,m}(\eta) \tilde{\psi}'_{f,n}(\eta) \tilde{\psi}'_{f,q}(\eta) d\eta \quad (\text{A.1.b})$$

$$A_{mnq} = A_{1,mnq} + A_{2,mnq} \quad (\text{A.1.c})$$

$$B_{mn} = \int_0^{\eta_f} \tilde{\psi}'_{f,m}(\eta) \left[\frac{\partial F_{\sim}}{\partial \eta} \tilde{\psi}'_{f,n}(\eta) - \frac{\partial^2 F_{\sim}}{\partial \eta^2} \tilde{\psi}'_{f,n}(\eta) \right] d\eta \quad (\text{A.1.d})$$

$$C_{mn} = \int_0^{\eta_f} \tilde{\psi}'_{f,m}(\eta) \left[\xi \frac{\partial^2 F_{\sim}}{\partial \xi \partial \eta} \tilde{\psi}'_{f,n}(\eta) - \xi \frac{\partial F_{\sim}}{\partial \xi} \tilde{\psi}'_{f,n}(\eta) + \frac{\partial F_{\sim}}{\partial \eta} \tilde{\psi}'_{f,n}(\eta) \right. \\ \left. - \frac{3}{4} F_{\sim} \tilde{\psi}'_{f,n}(\eta) - \frac{3}{4} \frac{\partial^2 F_{\sim}}{\partial \eta^2} \tilde{\psi}'_{f,n}(\eta) \right] d\eta \quad (\text{A.1.e})$$

$$\bar{g}_{f,m} = \int_0^{\eta_f} \tilde{\psi}'_{f,m}(\eta) \left\{ Sc\varphi_F + Sc \frac{\beta_T}{\beta_c} (T_{\infty} - T_w)\theta_F + \frac{3}{4} F_{\sim} \frac{\partial^2 F_{\sim}}{\partial \eta^2} - \frac{1}{2} \left(\frac{\partial F_{\sim}}{\partial \eta} \right)^2 - \xi \left[\frac{\partial F_{\sim}}{\partial \eta} \frac{\partial^2 F_{\sim}}{\partial \xi \partial \eta} - \frac{\partial F_{\sim}}{\partial \xi} \frac{\partial^2 F_{\sim}}{\partial \eta^2} \right] \right\} d\eta \quad (\text{A.1.f})$$

$$D_{mnq} = \int_0^{\eta_f} \tilde{\psi}'_{\theta\varphi,m}(\eta) \tilde{\psi}'_{f,n}(\eta) \tilde{\psi}'_{\theta\varphi,q}(\eta) d\eta \quad (\text{A.1.g})$$

$$E_{mnq} = - \int_0^{\eta_f} \tilde{\psi}'_{\theta\varphi,m}(\eta) \tilde{\psi}'_{f,n}(\eta) \tilde{\psi}'_{\theta\varphi,q}(\eta) d\eta \quad (\text{A.1.h})$$

$$G_{mn} = \int_0^{\eta_f} \frac{\partial F_{\sim}}{\partial \eta} \tilde{\psi}'_{\theta\varphi,m}(\eta) \tilde{\psi}'_{\theta\varphi,n}(\eta) d\eta \quad (\text{A.1.i})$$

$$H_{mn} = - \int_0^{\eta_f} \left[\xi \frac{\partial F_{\sim}}{\partial \xi} + \frac{3}{4} F_{\sim} \right] \tilde{\psi}'_{\theta\varphi,m}(\eta) \tilde{\psi}'_{\theta\varphi,n}(\eta) d\eta \quad (\text{A.1.j})$$

$$K_{mn} = - \int_0^{\eta_f} \frac{\partial \theta_F}{\partial \eta} \tilde{\psi}'_{\theta\varphi,m}(\eta) \tilde{\psi}'_{f,n}(\eta) d\eta \quad (\text{A.1.k})$$

$$L_{mn} = \int_0^{\eta_f} \tilde{\psi}'_{\theta\varphi,m}(\eta) \left[\xi \frac{\partial \theta_F}{\partial \xi} \tilde{\psi}'_{f,n}(\eta) - \frac{3}{4} \frac{\partial \theta_F}{\partial \eta} \tilde{\psi}'_{f,n}(\eta) \right] d\eta \quad (\text{A.1.l})$$

$$\bar{g}_{\theta,m} = \int_0^{\eta_f} \tilde{\psi}'_{\theta\varphi,m}(\eta) \left\{ \frac{3}{4} F_{\sim} \frac{\partial \theta_F}{\partial \eta} - \xi \left[\frac{\partial F_{\sim}}{\partial \eta} \frac{\partial \theta_F}{\partial \xi} - \frac{\partial F_{\sim}}{\partial \xi} \frac{\partial \theta_F}{\partial \eta} \right] \right\} d\eta \quad (\text{A.1.m})$$

$$O_{mn} = - \int_0^{\eta_f} \frac{\partial \varphi_F}{\partial \eta} \tilde{\psi}'_{\theta\varphi,m}(\eta) \tilde{\psi}'_{f,n}(\eta) d\eta \quad (\text{A.1.n})$$

$$P_{mn} = \int_0^{\eta_f} \tilde{\psi}'_{\theta\varphi,m}(\eta) \left[\xi \frac{\partial \varphi_F}{\partial \xi} \tilde{\psi}'_{f,n}(\eta) - \frac{3}{4} \frac{\partial \varphi_F}{\partial \eta} \tilde{\psi}'_{f,n}(\eta) \right] d\eta \quad (\text{A.1.o})$$

$$\bar{g}_{\varphi,m} = \int_0^{\eta_f} \tilde{\psi}'_{\theta\varphi,m}(\eta) \left\{ \frac{3}{4} F_{\sim} \frac{\partial \varphi_F}{\partial \eta} - \xi \left[\frac{\partial F_{\sim}}{\partial \eta} \frac{\partial \varphi_F}{\partial \xi} - \frac{\partial F_{\sim}}{\partial \xi} \frac{\partial \varphi_F}{\partial \eta} \right] \right\} d\eta \quad (\text{A.1.p})$$

APPENDIX B. INITIAL CONDITIONS

The initial conditions applied at a finite ξ can be written as,

$$\delta(10^{-6}) = \delta_0 = \left[\frac{c_{p,l}(T_\infty - T_w)}{Pr_l h_{fg}} \right]^{1/4} \left(\frac{g}{4\nu_l^2} \right)^{-1/4} 10^{-3/2} \quad (\text{B.1.a})$$

$$a_0(10^{-6}) = 10^{-6}; \quad \left. \frac{\partial f^*}{\partial \eta} \right|_{\xi=10^{-6}} = 10^{-6} \quad (\text{B.1.b,c})$$

$$\theta^*(10^{-6}, \eta) = 10^{-6}; \quad \varphi^*(10^{-6}, \eta) = 10^{-6} \quad (\text{B.1.d,e})$$

The transformed initial conditions are obtained by applying the operator $\int_0^{\eta_f} \tilde{\psi}'_{f,m}(\eta)(\cdot)d\eta$ to eq. (B.1.c) and $\int_0^{\eta_f} \tilde{\psi}'_{\theta\varphi,m}(\eta)(\cdot)d\eta$ to eqs. (B.1.d,e), yielding,

$$\bar{f}_m(10^{-6}) = 10^{-6} \int_0^{\eta_f} \tilde{\psi}'_{f,m}(\eta)d\eta \quad (\text{B.2.a})$$

$$\bar{\theta}_m(10^{-6}) = 10^{-6} \int_0^{\eta_f} \tilde{\psi}'_{\theta\varphi,m}(\eta)d\eta \quad (\text{B.2.b})$$

$$\bar{\varphi}_m(10^{-6}) = 10^{-6} \int_0^{\eta_f} \tilde{\psi}'_{\theta\varphi,m}(\eta)d\eta \quad (\text{B.2.c})$$

References

- [1] J.G. Collier, J.R. Thome, *Convective Boiling and Condensation*, fourth ed., Oxford University Press, Oxford, UK, 1994.
- [2] R. Senjaya, T. Inoue, Effects of non-condensable gas on the performance of oscillating heat pipe, part I: theoretical study, *Appl. Therm. Eng.* 73 (2014) 1387–1392, <https://doi.org/10.1016/j.applthermaleng.2014.02.074>.
- [3] R. Senjaya, T. Inoue, Effects of non-condensable gas on the performance of oscillating heat pipe, part II: experimental study, *Appl. Therm. Eng.* 73 (2014) 1393–1500, <https://doi.org/10.1016/j.applthermaleng.2014.02.075>.
- [4] J. Su, Z. Sun, G. Fan, M. Ding, Experimental study of the effect of non-condensable gases on steam condensation over a vertical tube external surface, *Nucl. Eng. Des.* 262 (2013) 201–208, <https://doi.org/10.1016/j.nucengdes.2013.05.002>.
- [5] M. Punetha, S. Khandekar, A CFD based modelling approach for predicting steam condensation in the presence of non-condensable gases, *Nucl. Eng. Des.* 324 (2017) 280–296, <https://doi.org/10.1016/j.nucengdes.2017.09.007>.
- [6] V.T. Shahu, S.B. Thombre, Air gap membrane distillation: a review, *J. Renew. Sustain. Energy* 11 (2019), 045901, <https://doi.org/10.1063/1.5063766>.
- [7] I. Haechler, H. Park, G. Schnoering, T. Gulich, M. Rohner, A. Tripathy, A. Milionis, T.M. Schutzius, D. Poulikakos, Exploiting radiative cooling for uninterrupted 24-hour water harvesting from the atmosphere, *Sci. Adv.* 7 (2021), eabf3978, <https://doi.org/10.1126/sciadv.abf3978>.
- [8] C.S. Sharma, C. Stamatopoulos, R. Suter, P.R. von Rohr, D. Poulikakos, Rationally 3D-textured copper surfaces for Laplace pressure imbalance-induced enhancement in dropwise condensation, *ACS Appl. Mater. Interfaces* 10 (2018) 29127–29135, <https://doi.org/10.1021/acsami.8b09067>.
- [9] R. Enright, N. Miljkovic, J.L. Alvarado, K. Kim, J.W. Rose, Dropwise condensation on micro- and nanostructured surfaces, *Nanoscale Microscale Thermophys. Eng.* 18 (2014) 223–250, <https://doi.org/10.1080/15567265.2013.862889>.
- [10] B. El Fil, G. Kini, S. Garimella, A review of dropwise condensation: theory, modeling, experiments, and applications, *Int. J. Heat Mass Tran.* 160 (2020), 120172, <https://doi.org/10.1016/j.ijheatmasstransfer.2020.120172>.
- [11] D.F. Othmer, The condensation of steam, *Ind. Eng. Chem.* 21 (1929) 576–583, <https://doi.org/10.1021/ie50234a018>.
- [12] D.G. Kroger, W.M. Rohsenow, Condensation heat transfer in the presence of a non-condensable gas, *Int. J. Heat Mass Tran.* 11 (1968) 15–26, [https://doi.org/10.1016/0017-9310\(68\)90060-4](https://doi.org/10.1016/0017-9310(68)90060-4).
- [13] H.K. Al-Diwany, J.W. Rose, Free convection film condensation of steam in the presence of non-condensing gases, *Int. J. Heat Mass Tran.* 16 (1973) 1359–1369, [https://doi.org/10.1016/0017-9310\(73\)90144-0](https://doi.org/10.1016/0017-9310(73)90144-0).
- [14] E.M. Sparrow, S.H. Lin, Condensation heat transfer in the presence of a noncondensable gas, *J. Heat Tran.* 86 (1964) 430–436, <https://doi.org/10.1115/1.3688714>.
- [15] W.J. Minkowycz, E.M. Sparrow, Condensation heat transfer in the presence of noncondensables, interfacial resistance, superheating, variable properties, and diffusion, *Int. J. Heat Mass Tran.* 9 (1966) 1125–1144, [https://doi.org/10.1016/0017-9310\(66\)90035-4](https://doi.org/10.1016/0017-9310(66)90035-4).
- [16] J.W. Rose, Condensation of a vapor in the presence of a non-condensing gas, *Int. J. Heat Mass Tran.* 12 (1969) 233–237, [https://doi.org/10.1016/0017-9310\(69\)90065-9](https://doi.org/10.1016/0017-9310(69)90065-9).
- [17] G. Zschaecck, T. Frank, A.D. Burns, CFD modelling and validation of wall condensation in the presence of non-condensable gases, *Nucl. Eng. Des.* 279 (2014) 137–146, <https://doi.org/10.1016/j.nucengdes.2014.03.007>.
- [18] R.M. Cotta, Hybrid numerical-analytical approach to nonlinear diffusion problems, *Numer. Heat Tran. Part B Fund.* 127 (1990) 217–226, <https://doi.org/10.1080/1040779900896174>.
- [19] R.M. Cotta, *Integral Transforms in Computational Heat and Fluid Flow*, first ed., CRC Press, Boca Raton, FL, 1993.
- [20] R.M. Cotta, Benchmark results in computational heat and fluid flow: the integral transform method, *Int. J. Heat Mass Tran.* 37 (1994) 381–394, [https://doi.org/10.1016/0017-9310\(94\)90038-8](https://doi.org/10.1016/0017-9310(94)90038-8).
- [21] M.D. Mikhailov, M.N. Ozisik, *Unified Analysis and Solutions of Heat and Mass Diffusion*, first ed., John Wiley & Sons, New York, NY, 1984.
- [22] A.J. Diniz, J.B. Aparecido, R.M. Cotta, Heat conduction with ablation in a finite slab, *Int. J. Heat Technol.* 8 (1990) 30–43.
- [23] M.A. Leal, H.A. Machado, R.M. Cotta, Integral transform solutions of transient natural convection in enclosures with variable fluid properties, *Int. J. Heat Mass Tran.* 43 (2000) 3977–3990, [https://doi.org/10.1016/S0017-9310\(00\)00023-5](https://doi.org/10.1016/S0017-9310(00)00023-5).
- [24] J.B. Aparecido, R.M. Cotta, M.N. Ozisik, Analytical solutions to two-dimensional diffusion type problems in irregular geometries, *J. Franklin Inst.* 326 (1989) 421–434, [https://doi.org/10.1016/0016-0032\(89\)90021-5](https://doi.org/10.1016/0016-0032(89)90021-5).
- [25] L.A. Sphaier, R.M. Cotta, Analytical and hybrid solutions of diffusion problems within arbitrarily shaped regions via integral transforms, *Comput. Mech.* 29 (2002) 265–276, <https://doi.org/10.1007/s00466-002-0339-6>.
- [26] I.F. Pinheiro, G. Puccetti, G.L. Morini, L.A. Sphaier, Integral transform analysis of microchannel fluid flow: irregular geometry estimation using velocimetry data, *Appl. Math. Model.* 90 (2021) 943–954, <https://doi.org/10.1016/j.apm.2020.09.035>.
- [27] H. Luz Neto, J.N.N. Quaresma, R.M. Cotta, Natural convection in three-dimensional porous cavities: integral transform method, *Int. J. Heat Mass Tran.* 45 (2002) 3013–3032, [https://doi.org/10.1016/s0017-9310\(02\)00015-7](https://doi.org/10.1016/s0017-9310(02)00015-7).
- [28] L.A. Sphaier, A. Barletta, M. Celli, Unstable mixed convection in a heated inclined porous channel, *J. Fluid Mech.* 778 (2015) 428–450, <https://doi.org/10.1017/jfm.2015.394>.
- [29] I.F. Pinheiro, H.L. Serrano, L.A. Sphaier, F.C. Peixoto, V.N.H. Silva, Integral transform analysis of heat and mass diffusion in chemically reacting systems with Michaelis-Menten kinetics, *Int. Commun. Heat Mass Tran.* 100 (2019) 20–26, <https://doi.org/10.1016/j.icheatmasstransfer.2018.10.003>.

- [30] C.P. Naveira-Cotta, M. Lachi, M. Rebay, R.M. Cotta, Experiments and simulations in transient conjugated conduction-convection-radiation, *Heat Tran. Res.* 41 (2010) 209–231, <https://doi.org/10.1615/HeatTransRes.v41.i3.20>.
- [31] J.S. Pérez-Guerrero, R.M. Cotta, Integral transform solution for the lid-driven cavity flow problem in streamfunction-only formulation, *Int. J. Numer. Methods Fluid.* 15 (1992) 399–409, <https://doi.org/10.1002/flid.1650150403>.
- [32] S.P.A. Paz, E.N. Macedo, J.N.N. Quaresma, R.M. Cotta, Eigenfunction expansion solution for boundary layer equations in cylindrical coordinates: simultaneously developing flow in circular tubes, *Numer. Heat Tran. Part A Appl.* 52 (2007) 1123–1149, <https://doi.org/10.1080/10407780701364445>.
- [33] E. Figueira da Silva, R.M. Cotta, Benchmark results for internal forced convection through integral transformation, *Int. Commun. Heat Mass Tran.* 23 (1996) 1019–1029, [https://doi.org/10.1016/0735-1933\(96\)00084-X](https://doi.org/10.1016/0735-1933(96)00084-X).
- [34] P.L.C. Lage, R.H. Rangel, Generalized integral transform solution for boundary layer over a sphere, *Int. J. Numer. Methods Fluid.* 18 (1994) 721–731, <https://doi.org/10.1002/flid.1650180802>.
- [35] M.A.H. Bolivar, R.M. Cotta, P.L.C. Lage, Integral transform solution of the laminar boundary layer problem for flow past two-dimensional and axisymmetric bodies, *Numer. Heat Tran.* 33 (1998) 779–797, <https://doi.org/10.1080/10407789808913966>.
- [36] J. Su, On the integral transform solution of laminar boundary layers with distributed suction, *Hybrid Methods Eng.* 1 (1999) 103–118, <https://doi.org/10.1615/HybMethEng.v1.i2.20>.
- [37] C.P. Naveira, M. Lachi, R.M. Cotta, J. Padet, Hybrid formulation and solution for transient conjugated conduction-external convection, *Int. J. Heat Mass Tran.* 52 (2009) 112–123, <https://doi.org/10.1016/j.ijheatmasstransfer.2008.05.034>.
- [38] W. Nusselt, Die oberflächenkondensation der Wasserdampfes, *Z. Ver. Deutsch. Ing.* 60 (1916) 541–569.
- [39] J.C.Y. Koh, E.M. Sparrow, J.P. Hartnett, The two-phase boundary layer in laminar film condensation, *Int. J. Heat Mass Tran.* 2 (1961) 69–82, [https://doi.org/10.1016/0017-9310\(61\)90015-1](https://doi.org/10.1016/0017-9310(61)90015-1).
- [40] R.C. Reid, J.M. Prausnitz, T.K. Sherwood, *The Properties of Gases and Liquids*, third ed., McGraw-Hill, New York, NY, 1977.
- [41] A. Bejan, *Convection Heat Transfer*, fourth ed., Wiley, New Jersey, NJ, 2013.
- [42] J.W. Ribeiro, R.M. Cotta, On the solution of nonlinear drying problems in capillary porous media through integral transformation of Luikov equations, *Int. J. Numer. Methods Eng.* 38 (1995) 1001–1020, <https://doi.org/10.1002/nme.1620380609>.
- [43] C.F.T. Matt, Transient response of general one-dimensional distributed system through eigenfunction expansion with an implicit filter scheme, *Appl. Math. Model.* 39 (2015) 2470–2488, <https://doi.org/10.1016/j.apm.2014.11.005>.
- [44] S. Wolfram, *Wolfram Mathematica 12.3*, Wolfram Research Inc., Champaign, IL, 2021.
- [45] P.N. Brown, A.C. Hindmarsh, L.R. Petzold, Consistent initial condition calculation for differential-algebraic systems, *SIAM J. Sci. Comput.* 19 (1998) 1495–1512, <https://doi.org/10.1137/S1064827595289996>.
- [46] D.R. Lide, *Handbook of Chemistry and Physics*, tenth ed., CRC Press, Boca Raton, FL, 2010.
- [47] P.T. Tsilingiris, Review and critical comparative evaluation of moist air thermophysical properties at the temperature range between 0 and 100 °C for engineering calculations, *Renew. Sustain. Energy Rev.* 83 (2018) 50–63, <https://doi.org/10.1016/j.rser.2017.10.072>.
- [48] K.C.R.F. Ferreira, K.M. Lisboa, On conjugated heat transfer problems involving film condensation in the presence of a non-condensable gas, in: 26th International Congress of Mechanical Engineering. Nov. 22-26 2021, COBEM, Florianópolis, SC, Brazil, 2021.